Available online at https://jcst.rsu.ac.th
Formerly Rangsit Journal of Arts and Sciences (RJAS)

Journal of Current Science and Technology, July-December 2019 JCST Vol. 9 No. 2, pp. 107-122

ISSN 2630-0583 (Print)/ISSN 2630-0656 (Online)

Numerical simulation of gas-solid flow in a cement precalciner using adaptive mesh refinement

Poncharoen Chanamai and Supasit Rodkwan*

Department of Mechanical Engineering, Faculty of Engineering, Kasetsart University, Bangkok 10900, Thailand

*Corresponding author; E-mail: fengcerm@gmail.com

Received 12 July 2019; Revised 19 November 2019; Accepted 20 November2019
Published online 21 December 2019

Abstract

A burning process is very critical in the clinker production of cement industry. The process consists of precalcination in precalciner and combustion in the combustion chamber. During precalcination, the amount of 97% calcium carbonate ($CaCO_3$) chemically decomposes into calcium oxide (CaO) and carbon dioxide (CO_2), resulting in lower energy consumption at the precalciner. Therefore, this research focuses on numerical simulation of gas-solid flow in a cement precalciner using adaptive mesh refinement. The geometrical models of both gas and solid phases were carried out for subsequent mathematical analysis. The Eulerian scheme with a turbulent model and Lagrangian scheme with discrete phase model (DPM) were then applied for gas and solid phases, respectively, through the computational fluid dynamics (CFD), using the adaptive mesh refinement (AMR). Various parameters, such as temperature, streamline, velocity vector and trajectory of pulverised coal/raw meal were numerically obtained. In the gas phase, the temperature profiles were found, the streamlines of tertiary air, raw meal air, and kiln gas were shown, as well as the velocity vectors of various layers were illustrated. In the solid phase, the trajectories of pulverised coal, raw meal, and a mixture of pulverised coal/raw meal were presented. In the gas-solid phase, both the streamline and trajectory of a mixture of air, pulverised coal, and raw meal were given. With a measurement access limitation in the cement plant, the model validation can be mainly carried out through temperature measurement in the gas phase which shows a good correlation within 6% discrepancy. Consequently, the developed AMR model, in this research, can be further used to improve precalcination efficiency and precalciner design.

Keywords*: *AMR, cement, CFD, DPM, numerical simulation, precalciner

1. Introduction

The cement production is one of the significant elements in the building construction industry. The proportion of the major global cement production in China, India, USA, Japan are 51.9%, 6.2%, 1.9%, 1.2%, respectively (The European Cement Association (CEMBUREAU), 2017). In Thailand, the cement industry consumes up to 60.69% of the non-metallic sector's overall energy consumption (Assawamartbunlue, Surawattanawan, & Luknongbu, 2019). Conventionally, the cement production process can be divided into three stages. First, the raw material preparation includes the processing of the quarry, which is initiated, and then transferred by dump trucks into the first and second raw material crushers, and stored in silos and raw material storages, respectively. After that, the raw materials are taken to the grinding mill and are sent to the homogenizing silo. This process is known as the raw meal preparation for a burning process. Next, in the burning process, the raw meal is fed into a preheater. The preheater consists of two sets, and each set includes six cyclones to eliminate humidity in the raw meal. The temperature of the preheater is between 200°C and 800°C. Then, the raw meal is sent to the precalciner, which functions as a secondary combustion. The fuel used are the pulverised coal and alternative fuel, which can be tire derived fuel (TDF), refuse derived fuel (RDF), and biomass fuel. The approximate temperature of raw meal is 800°C-1000°C. Then they are sent to the main burner, functioning as a primary combustion, which uses pulverised coal. The raw meal combustion is heated until 1,450°C, when they become clinker and then is cooled to 100°C. They are round shaped with 2.5 cm in diameter. Finally, they are kept in clinker storage. Lastly, in the finishing process, the clinker is fed to a finishing grinding mill and is combined with gypsum, and is then stored in the cement storage. Finally, they are

packed in cement bags for shipping. The whole cement production process is shown in Figure 1. The burning process is the most crucial in the cement production process, because there is an approximate fuel usage of 2.9-6.7 GJ per tonne of clinker or 20-25% of cement production, and 1.7 tonne clinker production per ton of raw materials. Moreover, there are 110-120 kWh of electricity usage per ton of cement (Oss & Padovani, 2003; Saidur, Hossain, Islam, Fayaz, & Mohammed, 2011; Rahman, Rasul, Khan, & Sharma, 2013).

The combustion systems are divided into two parts including a main burner or primary combustion that works in a stable condition, and precalciner or secondary combustion that is installed between the preheater and prior to the entrance of the main burner of the cement production process (Klotz, 1997), where 60% of pulverised coal is used in precalciner and around 40% is used in the main burner.

There are some advantages of precalciner in a cement industry. At present, the precalciners are smaller in overall dimensions which enable the burner to be more stable. This can lead to longer refractory life and reduction of NO_x, SO_3, Na, K, and Cl at the burning zone. In addition, various types and sizes of alternative fuel can be used. However, there are some limitations of precalciner which needs additional tertiary air duct equipment to carry out hot air from the clinker cooler into the precalciner. A chemical element, the reduction of NO_x and condensation of volatile alkalis remain a challenging problem because of the quality and quantity of raw materials and fuel. Furthermore, the control of combustion system and using alternative fuel can lead to temperature fluctuation because of the increase in the number of combustion systems (Holderbank Cement Seminar, 2000; Wikipedia, (n.d.); Heng, 1980).

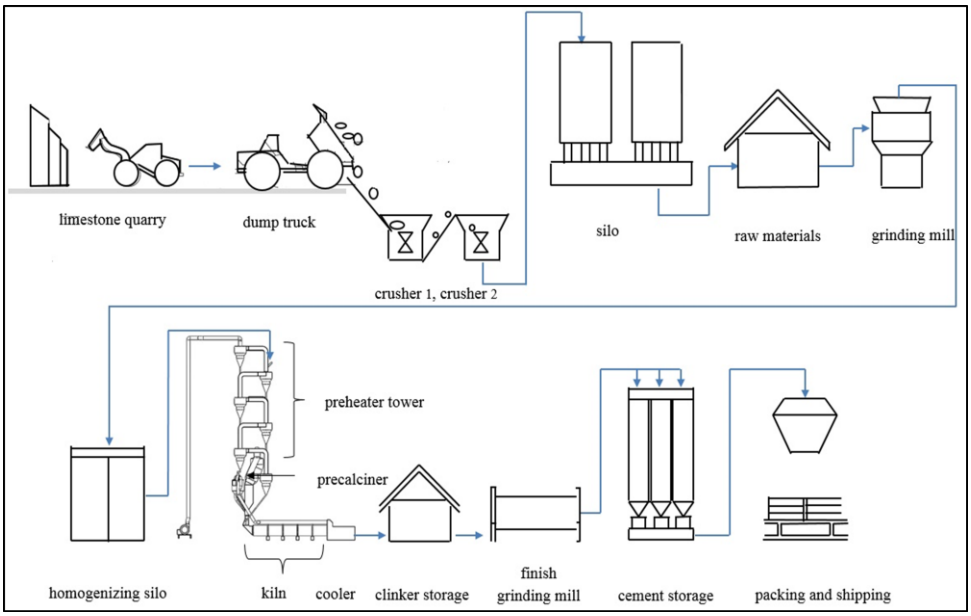

Figure 1 Schematic of cement production

As mentioned earlier, the precalciner plays an important role in cement production. Therefore, the understanding of cement production and precalciner is needed. The major topics of literature review are listed as follow:

First, for modeling of precalciner, Siwei et al. (2005) introduced a model of gas flow in the preheater and precalciner. The variables of the study are pressure drop and velocity. The study revealed that the preheater has a spiral flow, but the precalciner has a swirl flow. The velocity of the flow will affect the heat transfer between the gas-solid flows. However, if the velocity of the flow is decreased, the solid particles will adhere to the combustion chamber. Li, Ma, and Hu (2008) studied fluid dynamics of the precalciner by using model re-

normalization group, RNG. The study showed that the fluid dynamics consist of spiralled, sprayed zone, high zone and back-flow zone, which benefit the dispersion of raw meal and fuel. Ghizdavet, Volceanov, and Augustin (2008) investigated the gas velocity of the precalciner. The study revealed that the different velocity levels of gas affect the motion pattern of the same, which has a swirl flow inside the precalciner.

Second, for gas-solid flows, the previous study investigated the flow pattern inside the precalciner. The combustion chamber consists of raw meal and fuel which move with the flow of gas. There are many studies focusing on the gas-solid flows, combustion and the chemical reaction. Mei, Xie, He, and Jin (2012) and Mei, Xie, He, and Jin (2013) studied the position for coal fuel injection and raw meal to feed into the precalciner. The study revealed that the effective position for the coal fuel injection and raw meal occurs when the injection can cause combustion and decomposition of the raw meal. Mei et al. (2017) investigated the coupling coal combustion and calcium carbonate ($CaCO_3$) in the precalciner. They found that the mixed gas rose spirally and the volatile was initially released and burned. In addition, the study indicates the predicted burn-off rate of coal and decomposing rate of the $CaCO_3$. Huang, Lu, Xia, Li, and Ren (2006) developed a model of precalciner by CFD code Fortran 90 to predict the coal fuel and raw meal and to study the chemical reaction. The variables used in this study were velocity, temperature, concentration of O_2 and CO_2. The study also revealed that the swirling flow would affect the fuel and raw meal to flow in the combustion chamber for residence time. Kolyfetis and Vayenas (1988) had analysed and divided the fuel and raw meal into three parts: the heat transfer, pyrolysis and combustion. However, the study did not reveal any information about the gas-solid flows. Xie and Mei (2008) studied the model of the flow of gas and raw meal and found that the dispersion of raw meal was non-uniform and had back-flow in the wall. The study of Chen, Xie, Mei, and Shen (2016) was focusing on the motion patterns of the gas-solid flows, which are trajectory, coal, $CaCO_3$ and temperature and decomposition of $CaCO_3$. These caused a swirl in the combustion chamber. Even though Jiamei, Guoquan, and Baoguo (2006) studied gas-solid flows inside the precalciner, the velocity, temperature and trajectory of raw meal and coal, the study did not reveal much information about it. Moreover, Xing and Zhao (2011) had studied the model of gas-solid flows inside the precalciner and had predicted that there would be spray and swirl flows inside it. However, this study only focused on the motion of the gas-solid flows. Borawski (2009) researched the gas-solid flows and the effects of raw meal and motion pattern inside the combustion chamber. The research compared simulation and experiment. Furthermore, Hu, Lu, Huang, and Wang (2006); Luo (2011) had adjusted the various sizes of raw meal and coal to study the effects of fluid inside the precalciner. Xie and Mei (2007) studied the effects of adjusting the entry angle of raw meal into the precalciner and the dispersion of raw meal.

Third, for combustion and chemical reaction, Dou, Chen, and Huang (2009) studied the effects of combustion reaction and decomposition of the raw meal inside the precalciner. Giddings, Eastwick, Pickering, and Simmons (2000) also studied the combustion reaction of the coal fuel and raw meal and the motion pattern between the gas-solid flows inside the precalciner. Fidaros, Baxevanou, Dritselis, and Vlachos (2007) researched the gas-solid flows and calcination processes, which were affected by coal and pet coke fuel. The study revealed that the combustion of pet coke would increase the percentage of calcination processes more than the combustion of coal. In addition, Li, Ba, Egbert, and Cheng (2019) presented a numerical model to predict temperature, velocity, streamline of gas and trajectories of coal and raw meal as well as combustion process inside the industrial precalciner. This study shows that the gas spirals upward and the resulting vortices effectively disperse the particles and increase the residence time of raw meal and coal.

Fourth, for CFD simulation, numerical investigation, and environmental impacts, Huanpeng et al. (2004); Jianxiang, Tingzhi, and Jing (2012) analysed the model of precalciner by using the kinetic theory of granular flow (2-D) and unsteady state, which caused the particle-particle collisions. The variables in these studies are the velocity of gas-solid and the particle concentration. Chinyama, Lockwood, Yousif, and Kandamby (2008) emphasised on studying the $CaCO_3$ decomposition or calcination to find out the calcination level, and compare the result of simulation and the actual measurement. Mikulčić et al. (2012) studied the effects of raw meal injected by axial and swirl burner and the dispersion of raw meal and temperature inside the precalciner. Next, Huang, Lu, Hu, and Wang (2006) and Chen, Ye, and Gao (2011) studied

the effects of the precalciner by using CFD to analyse gases, such as NO_x, CO, O_2 and the behaviour of these gases. This study leads to the equipment improvement to reduce the amount of pollution. Mikulčić et al. (2012) focused on a thermal-chemical process in a precalciner and other various parameters such as temperature field, interaction gas-solid, and concentrations of reactants. The study revealed that, when the temperature in a precalciner is increased, the calcination rate is faster. Mikulčić et al. (2012) used CFD to analyze the thermo-chemical reactions in order to find a way to reduce CO_2. Among parameters studied include velocity, temperature, limestone, lime, CO_2, and CO mass fraction. The study showed that the mentioned parameters of the calcination process significantly affect CO_2 emission.

Finally, for investigation of alternative fuels, Mei, Xie, Chen, and He (2016) studied the use of alternative fuel such as coal and RDF in the precalciner. This study showed that the use of RDF severely weakens the initial combustion of coal, and further contributed to the fundamental understanding of coal-RDF's behavior. Mikulčić, Berg, Vujanović, and Duić (2014) proposed the use of biomass in a portion of 10%, 20%, and 30% on fossil fuels. They employed CFD analysis on a precalciner and various parameters, such as gas streamlines, temperature, CO_2 mole fraction, $CaCO_3$ and CaO mass fraction in particles were shown. Mtui (2013) investigated shredded tires and pine wood for use as alternative fuels. This study shows that up to 20% mixing of biomass and shredded tires can greatly increase the heat transfer rate.

2. Objectives

This research aims to perform numerical simulation of gas-solid flow in a cement precalciner with a complicated shape and pulverised coal using Eulerian and Lagrangian schemes through adaptive mesh refinement to obtain temperature, streamline, velocity vector, as well as coal/raw meal trajectories.

3. Materials and methods

3.1 Geometrical model

This study emphasises on studying the mathematical model to predict the behaviour of the process occurred inside the precalciner, as shown in Figure 2 (a) and Figure 2 (b). Figure 2 (c) shows a typical schematic of the burning process in the cement plant. It is noteworthy that the precalciner is located between cyclone (C2) and kiln inlet. In the gas phase, the primary air, consisting of the axial air and the swirl air, flows into the burner and swivel volute, the secondary air or kiln gas from the kiln, and the tertiary air from the clinker cooler are shown as Figure 3 (a). In the solid phase, the raw meal is passed into cyclones (C5 and C6), and then is fed through lower cyclones (C2-C4) for the preheating process before entering the precalciner. Also, the raw meal residue from precalciner is transported into the cyclone (C1) and kiln inlet. In addition, the pulverised coal enters into the burner and then the combustion chamber, as shown as Figure 3 (b).

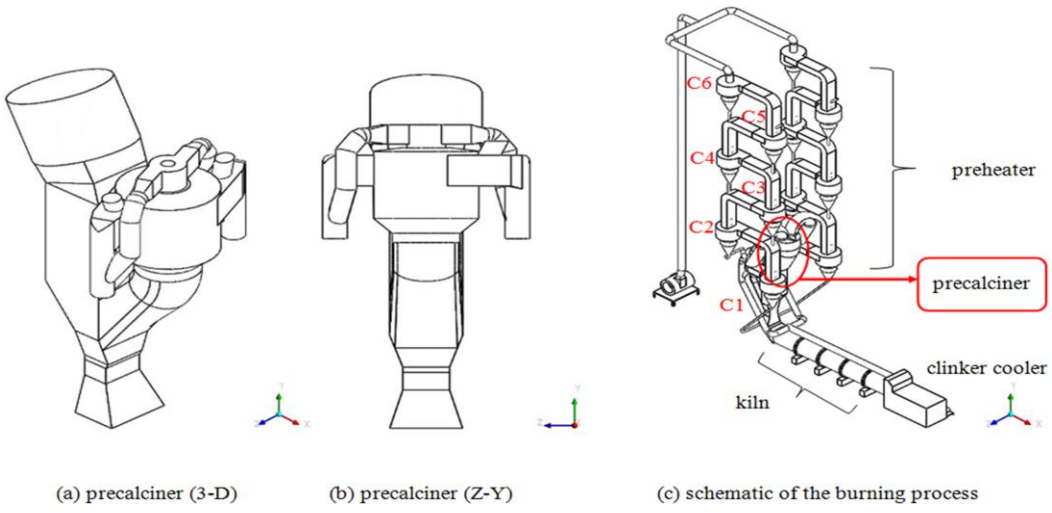

Figure 2 Precalciner for cement production industry: (a) precalciner 3-D; (b) precalciner (Z-Y); and (c) schematic of the burning process

JCST Vol. 9 No. 2 Jul.-Dec. 2019, pp. 107-122
ISSN 2630-0583 (Print)/ISSN 2630-0656 (Online)

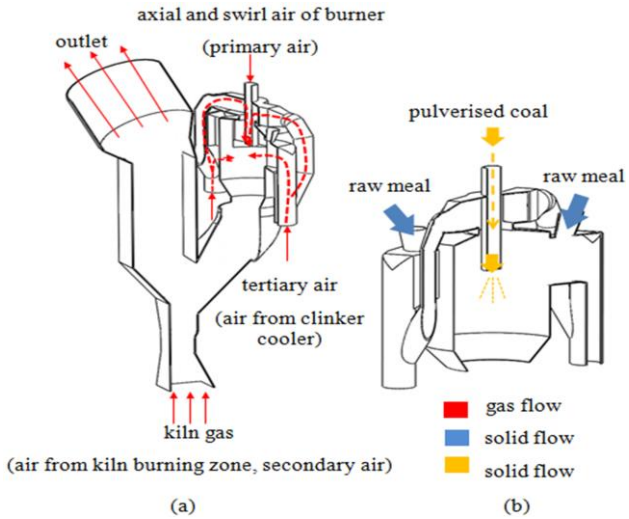

Figure 3 Schematic of gas-solid interaction in the precalciner: (a) Gas phase; and (b) Solid phase

3.2 Mathematic model

In this research, a precalciner model was developed mathematically using computational fluid dynamics (CFD). In gas phase, the Eulerian scheme for the gas phase, steady state and three dimensions fully developed the flow and incompressible flow with the Reynolds-averaged Navier-Stokes (RANS) equations, such as mass, momentum, and energy equations, with the realisable $k-\varepsilon$ turbulent model. The mass, momentum, and energy equation are presented in Eq. (1)-(3).

Mass equation

$$\frac{\partial}{\partial x_i}(\partial u_i) = 0 \tag{1}$$

Momentum equation

$$\frac{\partial}{\partial x_j}(\rho u_i u_j) = \frac{\partial p}{\partial x_i} + \frac{\partial}{\partial x_j}\left[\mu\left(\frac{\partial u_i}{\partial x_j} + \frac{\partial u_j}{\partial x_i}\right)\right] - \frac{\partial \rho \overline{u_i' u_j'}}{\partial x_j} \tag{2}$$

Energy equation

$$\frac{\partial}{\partial x_i}\left[u_i(\rho E + p)\right] = \frac{\partial}{\partial x_i}\left(k_{eff}\frac{\partial T}{\partial x_i}\right) \tag{3}$$

Where $x_i(i=x,y,z)$ denotes the Cartesian coordinates, and $u_i(u_x,u_y,u_z)$ denotes the Cartesian components of the velocity vector, ρ is the density, p is the pressure, μ is the fluid viscosity. T is the air temperature, k_{eff} is the effective conductivity, E is the total energy. Eq. (4) uses the Boussinesq hypothesis to determine the turbulence viscosity. Turbulent Eddy viscosity is shown in Eq. (5).

$$-\rho\overline{u_i' u_j'} = \mu_t\left(\frac{\partial u_i}{\partial x_j} + \frac{\partial u_j}{\partial x_i}\right) - \frac{2}{3}\left(\rho k + \mu_t\frac{\partial u_k}{\partial x_k}\right)\delta_{ij} \tag{4}$$

$$\mu_t = \rho C_\mu \frac{k^2}{\varepsilon} \tag{5}$$

3.2.1 Turbulence model

In this work, the turbulence model is simulated using the realisable two equation models. The turbulence kinetic energy (k) and turbulence dissipation rate (ε) models are shown in Eq. (6) and (7) (Shih, Liou, Shabbir, Yang, & Zhu 1995).

$$\frac{\partial}{\partial t}(\rho k)+\frac{\partial}{\partial x_j}(\rho k u_j)=\frac{\partial}{\partial x_j}\left[\left(\mu+\frac{\mu_t}{\sigma_k}\right)\frac{\partial k}{\partial x_j}\right]+G_k+G_b-\rho\varepsilon-Y_M+S_k \tag{6}$$

$$\frac{\partial}{\partial t}(\rho\varepsilon)+\frac{\partial}{\partial x_j}(\rho\varepsilon u_j)=\frac{\partial}{\partial x_j}\left[\left(\mu+\frac{\mu_t}{\sigma_\varepsilon}\right)\frac{\partial \varepsilon}{\partial x_j}\right]+\rho C_1 S\varepsilon-\rho C_2\frac{\varepsilon^2}{k+\sqrt{\upsilon\varepsilon}} + C_{1\varepsilon}\frac{\varepsilon}{k}C_{3\varepsilon}G_b+S\varepsilon \tag{7}$$

The model constants have the following default values, shown as Eq. (8) and Eq. (9).

$$C_1=\max\left[0.43,\frac{\eta}{\eta+5}\right],\eta=S\frac{k}{\varepsilon},S=\sqrt{2S_{ij}S_{ij}},\upsilon=\frac{\mu}{\rho} \tag{8}$$

$$C_{1\varepsilon}=1.44,C_2=1.92,\sigma_k=1,\sigma_\varepsilon=1.2,C_\mu=0.09,C_{3\varepsilon}=1 \tag{9}$$

In these equations, G_k is the generation of turbulent kinetic energy because of the mean velocity gradients, G_b is the generation of turbulence kinetic energy as a result of buoyancy, Y_M is the contribution of the fluctuating dilatation in compressible turbulence to the overall dissipation rate, c_2 and $c_{1\varepsilon}$ are constants, σ_k and σ_ε are the turbulent Prandtl numbers for k and ε, S_k and S_ε are user-defined source terms, υ is kinematic viscosity.

Where G_k, G_b, Y_M defined by Eq. (10)–Eq. (12)

$$G_k=-\rho\overline{u_i'u_j'}\frac{\partial u_j}{\partial x_i} \tag{10}$$

$$G_b=\beta g_i\frac{\mu_t}{\mathrm{Pr}_t}\frac{\partial T}{\partial x_i} \tag{11}$$

$$Y_M=2\rho\varepsilon M_t^2 \tag{12}$$

In solid phase, the Lagrangian scheme for solid phase and DPM were carried out with an assumption of neglected interaction among the spherical particles. This force balance equates the particle inertia with the force acting on the particle, and can be written as Eq. (13). The drag force is defined by Eq. (14). Additionally, the stochastic tracking method with discrete random walk (DRW) model was used for the solid dispersion, consisting of pulverised coal and raw meal.

$$\frac{du_p}{dt}=F_D\left(\vec{u}-\vec{u}_p\right)+\frac{\vec{g}\left(\rho_p-\rho\right)}{\rho_p}+\vec{F} \tag{13}$$

$$F_D=\frac{18\,\mu}{\rho_p d_p^2}\frac{C_D R_e}{24} \tag{14}$$

JCST Vol. 9 No. 2 Jul.-Dec. 2019, pp. 107-122
ISSN 2630-0583 (Print)/ISSN 2630-0656 (Online)

Where $\vec{F}$ is an additional acceleration (force/unit particle mass) term, $F_D\left(\vec{u}-\vec{u}_p\right)$ is the drag force per unit particle mass, $\vec{u}$ is the fluid phase velocity, $\vec{u}_p$ is the particle velocity, μ is the molecular viscosity of the fluid, ρ is the fluid density, ρ_p is the density of the particle, d_p is the particle diameter and R_e is the relative Reynolds number, which is defined as Eq. (15). The drag coefficient C_D for smooth particles can be taken from Eq. (16), where a_1, a_2 and a_3 are constants. (Morsi & Alexander, 1972).

$$\mathrm{Re} \equiv \frac{\rho d_p \left|\overrightarrow{u_p} - \vec{u}\right|}{\mu} \tag{15}$$

$$C_D = a_1 + \frac{a_2}{R_e} + \frac{a_3}{R_e^2} \tag{16}$$

In the gas-solid phase, the volume fraction is a key parameter in determining the type of coupling resulting in different equations (Michaelides, Crowe, & Schwarzkopf, 2017). For example, the two-way coupling involves momentum and heat exchange equations defined by Eq. (17) and (18).

Momentum exchange,

$$F = \sum \left(\frac{18\,\mu C_D R_e}{\rho_p d_p^2 24}\left(u_p - u\right) + F_{vm} \right) \dot{m}_p \,\Delta t \tag{17}$$

Where μ is viscosity of the fluid, ρ_p is the density of the particle, d_p is the diameter of the particle, R_e is relative Reynolds number, u_p is velocity of the particle, u is velocity of the fluid, C_D is the drag coefficient, $\dot{m}_p$ is the mass flow rate of the particles, Δt is time step and F_{vm} is virtual mass force.

Heat exchange,

$$Q = \frac{\dot{m}_{p,0}}{m_{p,0}} \left[\left(m_{P_{in}} - m_{P_{out}}\right)\left[-H_{lat_{ref}} + H_{pyrol}\right] - m_{P_{out}} \int_{T_{ref}}^{T_{P_{out}}} c_{p_p}\, dT + m_{p_{in}} \int_{T_{ref}}^{T_{P_{in}}} c_{p_p}\, dT \right] \tag{18}$$

Where $\dot{m}_{p,0}$ is the initial mass flow rate of the particle injection, $m_{p,0}$ is the initial mass of the particle, $m_{p_{in}}$ is the mass of the particle on cell entry, $m_{p_{out}}$ is the mass of the particle on cell exit, c_{p_p} is the heat capacity of the particle, $T_{p_{in}}$ is the temperature of the particle on cell entry, $T_{p_{out}}$ is the temperature of the particle on cell exit, T_{ref} is the reference temperature for enthalpy, H_{pyrol} is the heat of pyrolysis as volatiles are evolved and $H_{lat_{ref}}$ is the latent heat at reference conditions.

3.3 Boundary conditions, numerical method, and meshing

The boundary conditions for the gas and solid phases, from a cement plant partnering with this research, used in this work are shown in Tables 1-3, respectively. In the gas phase, uniform velocity profiles of the tertiary air, raw meal air, and kiln gas are assumed at the inlet position. For the outlet position, pressure is under ambient atmosphere. Additionally, adiabatic process is given at the precalciner wall. The measured temperatures at the flame burner using infrared thermometer as well as at an entrance of the inlet kiln using thermocouple sensor are found. In the solid phase, particle shape is a smooth sphere. The wall boundary condition is a reflected type and the inlet and outlet boundaries are assumed to be escaped types.

The finite volume method (FVM) through differencing scheme of the semi-implicit method for pressure-linked equations (SIMPLE) algorithm was also represented. In this research, AMR was used to improve the quality, especially in the area where the mesh was not sufficient.

Table 1 Boundary conditions for gas phase

Type	Velocity (m/s)	Temperature (°C)
Tertiary air inlet (L-R)	35.87	905
Raw meal air inlet (L-R)	21.9	810
Kiln gas inlet	17	880
Axial air inlet	19.9	60
Swirl air inlet	60	1300

Table 2 Boundary conditions for solid phase

Type	Velocity (m/s)	Temperature (°C)
Pulverised coal	19.9	60
Raw meal	21.9	810

Table 3 Material properties

Type	Density (kg/m^3)	Specific heat (J/kg.K)	Mass flow rate (kg/s)	Dimension (μm)
Pulverised coal	1400	1680	8.33	90
Raw meal	2800	856	14.05	90

4. Results and discussion

4.1 Mesh verification model

In the mesh verification model, regular meshing was created by the tetrahedron type for 874,636 cells. It was found that the conventional method consumed for a long period of time. Therefore, the AMR method was introduced to obtain the solution in the area where the mesh was insufficient. Then, both solutions were compared on the temperature profile of the gas phase at a burner and an outlet of precalciner as shown in Figure 4 and Figure 5, respectively. It can be seen that the AMR solution is converged after adaptive mesh refinement No.6; therefore, the amount of 1,209,344 meshing cells was selected as shown in Figure 4. All AMR contours through temperature profile were shown in Figure 6.

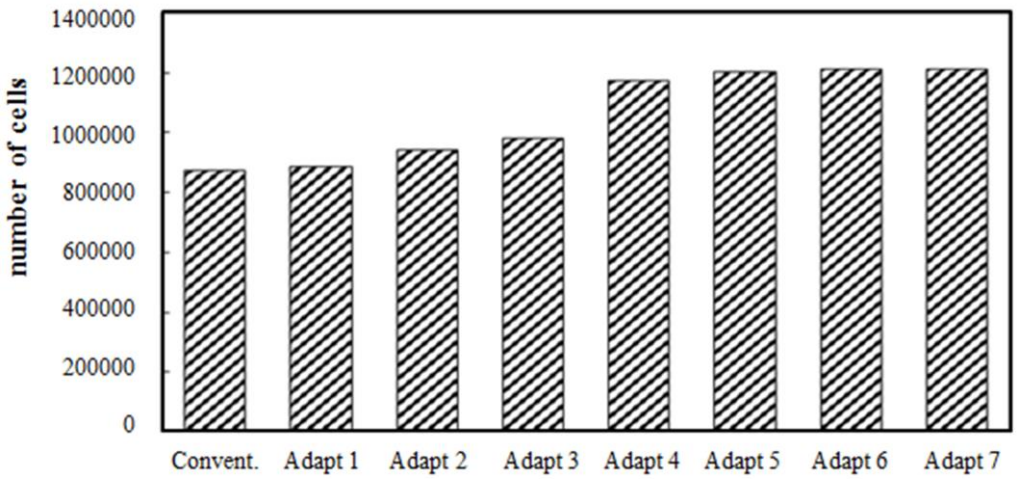

Figure 4 Number of adaptions

JCST Vol. 9 No. 2 Jul.-Dec. 2019, pp. 107-122
ISSN 2630-0583 (Print)/ISSN 2630-0656 (Online)

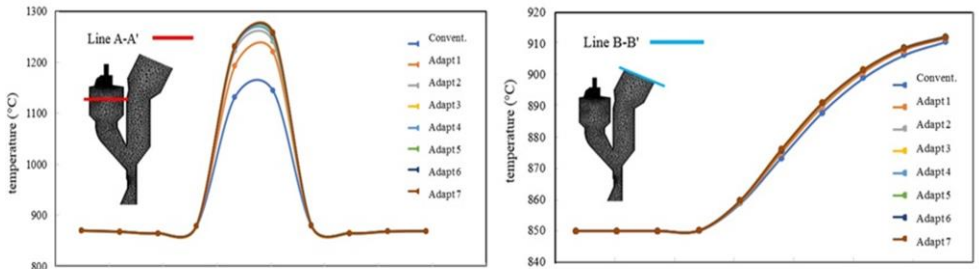

(a) (b)

Figure 5 Solution of temperature gradient: (a) a burner (line A-A') and (b) an outlet (line B-B')

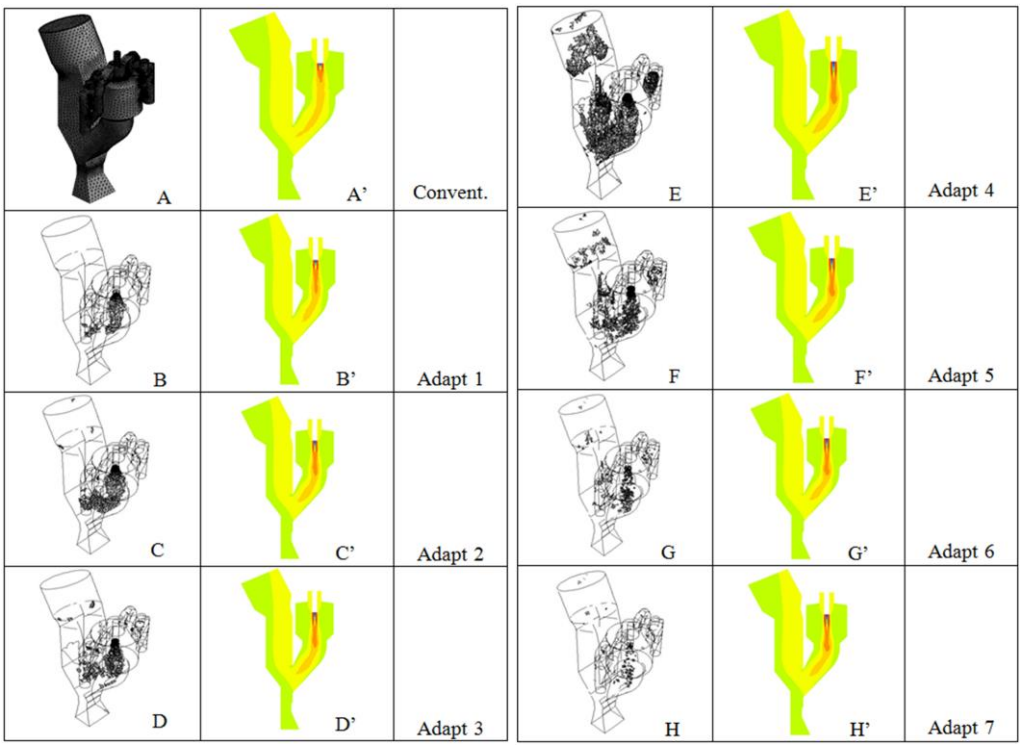

Figure 6 AMR contour through temperature profile of gas phase at a burner and an outlet of a precalciner

4.2 Gas phase

The profiles of temperature, streamline, and velocity vector in the precalciner were presented based on the given boundary conditions.

4.2.1 Temperature

Figure 7 shows the temperature gradient in the precalciner. The heat source at the swirl air inlet leads to the high temperature distribution of 1100°C-1300°C at the vicinity near the inlet, and then lower temperature in the range of 800°C-900°C at the bottom of the precalciner. The results correlate well with previous studies (Mikulčić, Berg, Vujanović, & Duić, 2014).

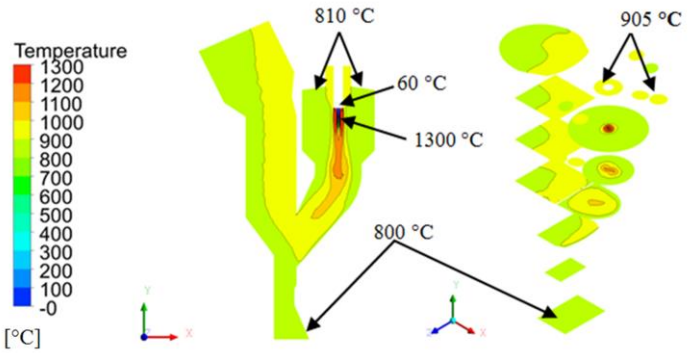

(a) (b)

Figure 7 Temperature profiles of the gas phase in a precalciner: (a) contour plot; and (b) slice plot

4.2.2 Streamline

The gas flow patterns of the tertiary air, raw meal air, and kiln gas were observed to determine the streamline characteristic. Figure 8 (a) shows the gas streamline from the tertiary air inlet. It is observed that the three flow patterns have existed: mixing and strong swirling, smooth swirling and smooth flow. In the mixing and strong swirling region, the raw meal air and the tertiary air is mixed inside the precalciner, under the eccentric tertiary inlet and raw meal inlets, resulting in an increasing swirl. In the smooth swirling, less turbulence is occurred during the gas moving down to the bottom of the precalciner. In the smooth flow, uniform gas streamline is found along the path through the outlet. Similar streamline pattern of the raw meal air, as seen in the tertiary air with three various stages of mixing and strong swirling, the smooth swirling and smooth flows are shown in Figure 8 (b). The kiln gas streamline from the rotary kiln moves uniformly upwards to the outlet, as shown in Figure 9 (a). In addition, the streamlines from tertiary air, raw meal air, and kiln gas are simultaneously depicted in Figure 9 (b). Additional flow pattern can be found at the transition point from swirling to uniform flow. Therefore, the important streamline characteristics were mixing and strong swirling which greatly affect the calcination and heat transfer during the gas-solid phase. The result shows good agreement with other research work (Mikulčić, Berg, Vujanović, & Duić, 2014).

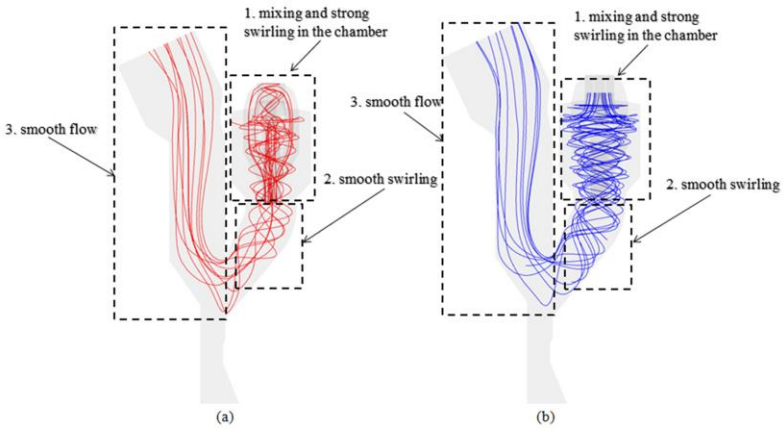

Figure 8 Streamline of the gas phase: (a) tertiary air; and (b) raw meal air

JCST Vol. 9 No. 2 Jul.-Dec. 2019, pp. 107-122
ISSN 2630-0583 (Print)/ISSN 2630-0656 (Online)

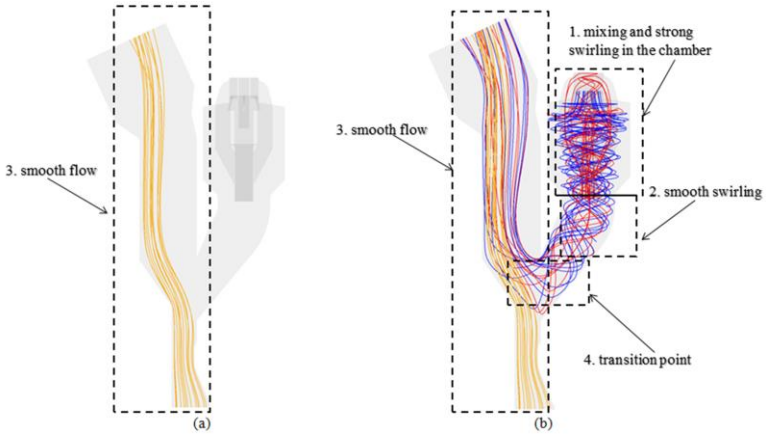

Figure 9 Streamline of the gas phase: (a) kiln gas; and (b) Mixing of all gas

4.2.3 Velocity

The velocity profile, velocity contour and velocity vector of all streamlines from tertiary air, raw meal air, and kiln gas are shown in Figure 10. It presents a similar tendency of swirling and uniformity in each region as occurred in the streamline pattern.

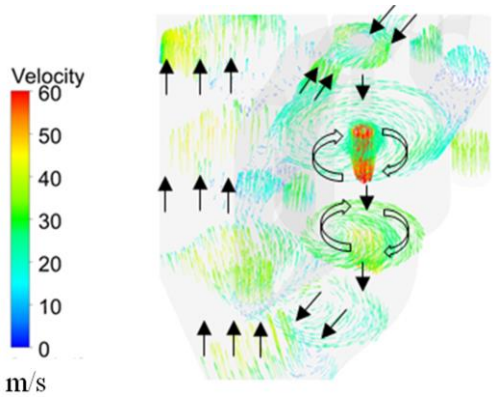

Figure 10 Vector velocity of the gas phase in the precalciner

4.3 Solid phase

4.3.1 Trajectories

Figure 11 (a) shows a trajectory of the pulverised coal injected from a burner into the combustion chamber and the outlet. The smooth flow pattern was found without swirling. The raw meal was injected from ducts of the cyclone to the chamber, as shown in Figure 11 (b). The mixing and strong swirling pattern leading to the extended residence time, and improved decomposition and calcination processes were exhibited. Figure 12 (a) also displays a combination of the pulverised coal and raw meal trajectories.

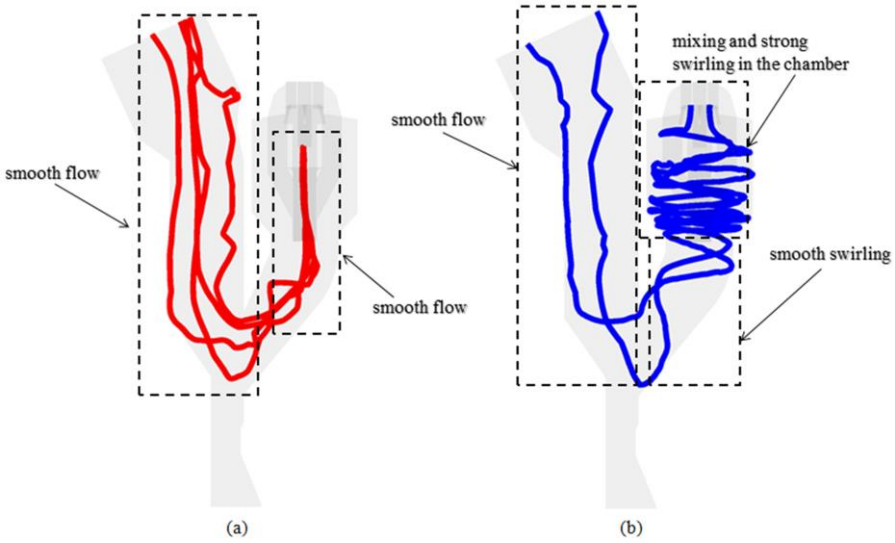

Figure 11 Trajectories of solid phase in the precalciner: (a) pulverised coal; and (b) raw meal

4.3.2 Temperature

Figure 12 (b) shows temperature profile of the pulverised coal, raw meal, and a mixing of pulverised coal and raw meal. The temperature intervals of the pulverised coal and raw meal were found to be 1000°C-1300°C and 800°C-1000°C, respectively.

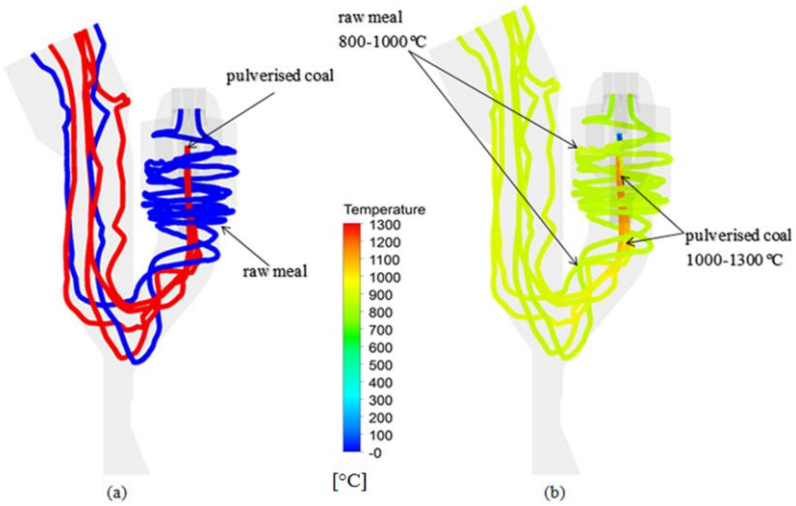

Figure 12 Mixing of trajectories and temperature of pulverised coal and raw meal: (a) Mixing of trajectories; and (b) temperature of pulverised coal and raw meal

4.4 Mixture of gas-solid phase

Finally, a mixture of the gas-solid streamline and trajectories, including tertiary air, raw meal air, kiln gas, pulverised coal, and raw meal is shown in Figure 13. The model developed in this work was mainly validated with temperature experimental data due to limited access of plant measurement. The result shows a good correlation within 6% discrepancy as shown in Table 4.

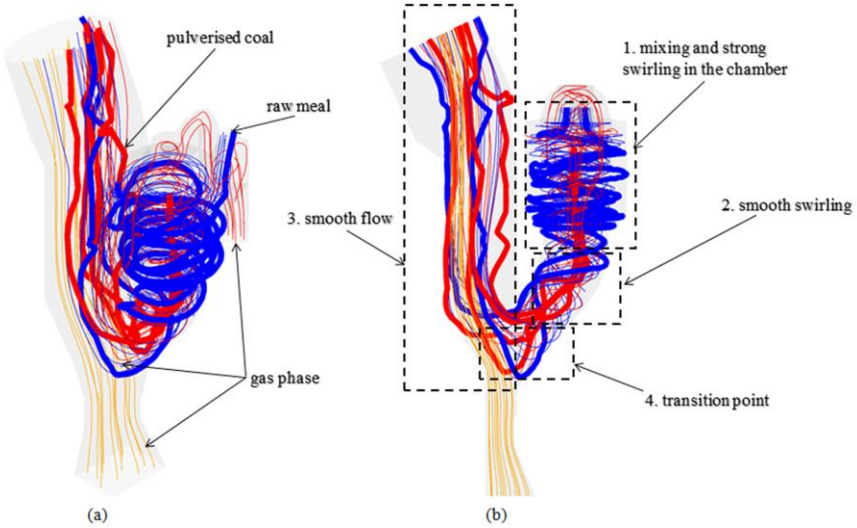

Figure 13 Mixing of streamline and trajectories of the gas-solid phase

Table 4 Verification of temperature

Parameters	Simulated temperature (°C)	Measured temperature (°C)	Percent Difference %
Flame burner	1283	1300	1.30
Kiln Inlet	880	835	5.38

5. Conclusion

In this research, a numerical simulation of gas-solid flow in a cement precalciner with a complicated shape and pulverised coal using adaptive mesh refinement, AMR, was performed. The geometrical models and mathematical analysis for gas and solid phases were adopted. The CFD simulation using AMR was applied with the Eulerian scheme, with turbulent model and Lagrangian scheme, with DPM. Various parameters, such as temperature, streamline, velocity vector and trajectory of pulverised coal/raw meal were numerically obtained for gas and solid phases and were then verified with temperature experimental data for model accuracy. Finally, the model validation through temperature measurement in the gas phase shows a good agreement within 6% discrepancy. Consequently, the model developed in this work can be used as another important tool to analyze the precalciner performance, and to improve the precalcination process for better efficiency and more productivity.

6. Acknowledgements

The funding of this research is mainly supported by Energy Policy and Planning Office (EPPO), Thailand, Ministry of Energy. The authors also would like to thank TPI Polene Company Limited for technical support on the cement plant and kind cooperation in this work.

7. References

Assawamartbunlue, K., Surawattanawan, P., & Luknongbu, W. (2019). Specific energy consumption of cement in Thailand. *Energy Procedia, 156*, 212-216. DOI: 10.1016/j.egypro.2018.11.130

Borawski, K. (2009). *Numerical investigation of gas-solid flow in the calciner.* A thesis for the degree of Master of Engineering in Thermal Energy and Process Engineering. AALBORG University, Copenhagen, Denmark.

Chen, X., Xie, J., Mei, S., & Shen, S. (2016). Numerical simulation of gas-solid flow and pulverized coal combustion in a swirl chamber precalciner. *Proceedings of the 2016 6th International Conference on Advanced Design and Manufacturing Engineering (ICADME 2016)*. DOI: 10.2991/icadme-16.2016.47

Chen, Z. B., Ye, F., & Gao, C. (2011). Numerical simulation of NSP cement NOx formation and control technology. *Advanced Materials Research, 356-360*, 1605-1608. DOI: 10.4028/www.scientific.net/amr.356-360.1605

Chinyama, M. P., Lockwood, F. C., Yousif, S. Y., & Kandamby, N. (2008). Modelling of calcium carbonate decomposition in cement plant precalciners. *Journal of the Energy Institute, 81*(1), 19-24. DOI: 10.1179/174602208x269355.

Dou, H., Chen, Z., & Huang, J. (2009, February). Numerical study of the coupled flow field in a double-spray calciner. *2009 International Conference on Computer Modeling and Simulation*. Macau, China. DOI: 10.1109/iccms.2009.45

Fidaros, D., Baxevanou, C., Dritselis, C., & Vlachos, N. (2007). Numerical modelling of flow and transport processes in a calciner for cement production. *Powder Technology, 171*(2), 81-95. DOI: 10.1016/j.powtec.2006.09.011

Ghizdavet, Z., Volceanov, A., & Semenescu, A. (2008). CFD Simulations of gases flow in calciners. *Revista de Chimie -Bucharest- Original Edition, 59*(5), 511-514. Retrieved May 1, 2019, from http//www.researchgate.net/publication/288011426_CFD_Simulations_of_gases_flow_in_calciners

Giddings, D., Eastwick, C. N., Pickering, S. J., & Simmons, K. (2000). Computational fluid dynamics applied to a cement precalciner. *Proceedings of the Institution of Mechanical Engineers, Part A: Journal of Power and Energy, 214*(3), 269-280. DOI: 10.1243/0957650001538353

Heng, S. Tao. (1980). Some interesting features of precalcining system. *World cement technology, 11*(7), 353-366. Retrieved May 1, 2019, from http//www.hstao.com/Cement/English/Interesting%20Precalcining%20Systems.pdf

Holderbank Cement Seminar. (2000). Materials technology I – Raw materials supply for cement and aggregate industry. Retrieved from https://archive.org/stream/HolderbankCementEngineeringBook/Pg_20602101_precalciningSystems#page/n5/mode/2up

Hu, Z., Lu, J., Huang, L., & Wang, S. (2006). Numerical simulation study on gas–solid two-phase flow in pre-calciner. *Communications in Nonlinear Science and Numerical Simulation, 11*(3), 440-451. DOI: 10.1016/j.cnsns.2004.07.004

Huang, L., Lu, J., Hu, Z., & Wang, S. (2006). Numerical simulation and optimization of NO emissions in a precalciner. *Energy & Fuels, 20*(1), 164-171.DOI: 10.1021/ef0502857

Huang, L., Lu, J., Xia, F., Li, W., & Ren, H. (2006). 3-D mathematical modeling of an in-line swirl-spray precalciner. *Chemical Engineering and Processing: Process Intensification, 45*(3), 204-213. DOI: 10.1016/j.cep.2005.09.001

Huanpeng, L., Wentie, L., Jianxiang, Z., Ding, J., Xiujian, Z., & Huilin, L. (2004). Numerical study of gas?solid flow in a precalciner using kinetic theory of granular flow. *Chemical Engineering Journal, 102*(2), 151-160. DOI: 10.1016/s1385-8947(04)00129-9

Jiamei, W., Guoquan, X., & Baoguo, M. (2006). Numerical simulation of the gas-solid two-phase flows in a precalciner. *Journal of Wuhan University of Technology-Mater. Sci. Ed., 21*(4), 177-179. DOI: 10.1007/bf02841233

Jianxiang, Z., Tingzhi, Y., & Jing, Y. (2012). Numerical simulation of gas and solid flow behavior in the pre-calciner with large eddy simulation approach. *Energy Procedia, 17*(Part B), 1535-1541. DOI:10.1016/j.egypro.2012.02.278

Klotz, B. (1997, April). New developments in precalciners and preheaters. 1997 IEEE/PCA Cement Industry Technical Conference. XXXIX Conference Record (Cat. No.97CH36076). Hershey, PA, USA. DOI: 10.1109/citcon.1997.599349

Kolyfetis, E., & Vayenas, C. G. (1988). Mathematical modelling of separate line precalciners (SLC). *ZKG International Research Manufacture Application*, *11*, 559-563. Retrieved June 3, 2019, from https://www.researchgate.net/publication/289526602_Mathematical_Modelling_of_separate_line_precalciners_SLC

Li, X., Ba, Q., Egbert, S., & Cheng, L. (2019). Measurements and modeling of fluid flow and thermal processes in an industrial precalciner. *Frontiers in Heat and Mass Transfer (FHMT), 12*. DOI: 10.5098/hmt.12.20

Li, X., Ma, B., & Hu, Z. (2008). Computational modeling of aerodynamic characteristics in sprayed and spiraled precalciner. *Communications in Nonlinear Science and Numerical Simulation, 13*(6), 1205-1211. DOI: 10.1016/j.cnsns.2006.10.002

Luo, H. (2011). Modeling the gas-solid flow in calcining furnace. *The Journal of Computational Multiphase Flows, 3*(1), 1-12. DOI: 10.1260/1757-482x.3.1.1

Mei, S., Xie, J., Chen, X., & He, F. (2016). Moving characteristics of coal and RDF in a swirl-type precalciner by numerical simulation. *Proceedings of the 2016 6th International Conference on Advanced Design and Manufacturing Engineering (ICADME 2016).* DOI: 10.2991/icadme-16.2016.49

Mei, S., Xie, J., Chen, X., He, F., Yang, H., & Jin, M. (2017). Numerical simulation of the complex thermal processes in a vortexing precalciner. *Applied Thermal Engineering, 125*, 652-661. DOI: 10.1016/j.applthermaleng.2017.07.041

Mei, S. X., Xie, J. L., He, F., & Jin, M. F. (2012). Numerical simulations of combustion and decomposition processes in precalciner with two types of locations of jetting coal pipes. *Applied Mechanics and Materials, 235*, 428-433. DOI: 10.4028/www.scientific.net/amm.235.428

Mei, S. X., Xie, J. L., He, F., & Jin, M. F. (2013). Numerical simulations of combustion and decomposition processes in precalciner with two different heights of raw meal inlets. *Applied Mechanics and Materials, 268-270*, 477-482. DOI: 10.4028/www.scientific.net/amm.268-270.477

Michaelides, E. E., Crowe, C. T., & Schwarzkopf, J. D. (2017). Multiphase flow handbook. Updated 2nd Edition. Boca Raton: CRC Press/Taylor & Francis Group.

Mikulčić, H., Berg, E. V., Vujanović, M., & Duić, N. (2014). Numerical study of co-firing pulverized coal and biomass inside a cement calciner. *Waste Management & Research, 32*(7), 661-669. DOI: 10.1177/0734242x14538309

Mikulčić, H., Berg, E. V., Vujanović, M., Priesching, P., Perković, L., Tatschl, R., & Duić, N. (2012). Numerical modelling of calcination reaction mechanism for cement production. *Chemical Engineering Science, 69*(1), 607-615. DOI: 10.1016/j.ces.2011.11.024

Mikulčić, H., Berg, E. V., Vujanović, M., Priesching, P., Tatschl, R., & Duić, N. (2012). CFD analysis of a cement calciner for a cleaner cement production. *Chemical Engineering Transactions, 29*, 1513-1518. Retrieved June 01, 2019, from http://https://core.ac.uk/download/pdf/34008106.pdf

Mikulčić, H., Vujanović, M., Fidaros, D. K., Priesching, P., Minić, I., Tatschl, R., . . . Stefanović, G. (2012). The application of CFD modelling to support the reduction of CO2 emissions in cement industry. *Energy, 45(1), 464-473*. DOI: 10.1016/j.energy.2012.04.030

Morsi, S. A., & Alexander, A. J. (1972). An investigation of particle trajectories in two-phase flow systems. *Journal of Fluid Mechanics, 55*(02), 193-208. DOI: 10.1017/s0022112072001806

Mtui, P. (2013). CFD modeling of devolatilization and combustion of shredded tires and pine wood in rotary cement kilns. *American Journal of Energy Engineering, 1*(5), 51-55. DOI: 10.11648/j.ajee.20130105.11

Oss, H. G., & Padovani, A. C. (2003). Cement manufacture and the environment part II: Environmental challenges and opportunities. *Journal of Industrial Ecology, 7*(1), 93-126. DOI: 10.1162/108819803766729212

Rahman, A., Rasul, M., Khan, M., & Sharma, S. (2013). Impact of alternative fuels on the cement manufacturing plant performance: An overview. *Procedia Engineering, 56*, 393-400. DOI: 10.1016/j.proeng.2013.03.138

Saidur, R., Hossain, M., Islam, M., Fayaz, H., & Mohammed, H. (2011). A review on kiln system modeling. *Renewable and Sustainable Energy Reviews, 15*(5), 2487-2500. DOI: 10.1016/j.rser.2011.01.020

Shih, T., Liou, W. W., Shabbir, A., Yang, Z., & Zhu, J. (1995). A new k-ϵ eddy viscosity model for high reynolds number turbulent flows. *Computers & Fluids, 24*(3), 227-238. DOI: 10.1016/0045-7930(94)00032-t

Siwei, C., Zuobing, C., Haijian, D., Jianxin, P., Jiquan, H., & Yawei, C. (2005). The numerical simulation of the flow field in a cold model of five-stage cyclone preheater and precalciner system. *Journal of Wuhan University of Technology-Mater. Sci. Ed., 20*(2), 99-101. DOI: 10.1007/bf02838501

The European Cement Association. (2017). Activity report 2017. CEMBUREAU, Rue d'Arlon 55 – BE-1040 Brussels, Belgium. Retrieved from https://cembureau.eu/media/1716/activity-report-2017.pdf

Wikipedia. (n.d.). Cement kiln. Retrieved 2019, May 03 from https://en.wikipedia.org/wiki/Cement_kiln

Xie, J., & Mei, S, (2007). Numerical simulation of gas-solid flow in SLC-S precalciner by adding a raw meal inlet. *Kuei Suan Jen Hsueh Pao/ Journal of the Chinese Ceramic Society, 35*(10), 1382-1386. Retrieved June 3, 2019, from https://www.researchgate.net/publication/289290304_Numerical_simulation_of_gas-solid_flow_in_SLC-S_precalciner_by_adding_a_raw_meal_inlet

Xie, J. L., & Mei, S. X. (2008). Numerical simulation of gas-solid flow in a precalciner of cement industry. *Materials Science Forum, 575-578*, 1234-1239. DOI: 10.4028/www.scientific.net/msf.575-578.1234

Xing, N. N., & Zhao, W. L. (2011). Numerical simulation of the gas-solid two-phase flow in the cement precalciner based on fluent software. *Advanced Materials Research, 255-260*, 4232-4236. DOI: 10.4028/www.scientific.net/amr.255-260.4232